Lab on a Chip

PAPER

View Article Online
View Journal

Cite this: DOI: 10.1039/d5lc00349k

Kappa(κ)Chip: a modular microfluidic device for analyte screening using parallelized assays and a multiple shear rate approach

Jose A. Wippold, *[a] Mark T. Kozlowski, [a] Joseph La Fiandra,[b] Jessica Boetticher,[b] Alison Grafton,[b] Justin P. Jahnke[a] and Joshua A. Orlicki[a]

Polymers are ubiquitous in the modern world, but many have low surface energies, making it difficult to engineer adhesive interactions with them. The large sequence space afforded by biology, along with its ability to evolve novel solutions to challenging problems, makes exploring bioinspired materials for novel adhesives attractive. However, the discovery of biologically-inspired adhesive modalities demands the development of high-throughput screening methods that use only small amounts of material, making microfluidics an ideal solution. In this work, we present the development of a novel microfluidic chip, the kappa(κ)Chip, which represents a significant leap in testing efficiency. The parallelized design of the kappa(κ)Chip enables 24 simultaneous adhesion tests from a single-input stream. This drastically reduces experimental time and reagent consumption, allowing for more comprehensive datasets and the ability to quickly compare the performance of multiple proteins against different substrates—a capability unavailable with current single-test platforms. The chip was used to evaluate the adhesive properties of fungal hydrophobin proteins engineered for display on the surface of cells, using the adhesion of the cells as a proxy for the ability of hydrophobins to serve as an adhesive. The device combines microfabrication, microfluidics, material sciences, synthetic biology, multiphysics simulation and ML in a unique way to enable the discovery of strong biological adhesives. The rapid screening capability of the kappa(κ)Chip facilitates an informed rank-ordering of potential binding motifs or sequences against arbitrary substrates. Moreover, this platform holds potential for applications in investigating cell adhesion in tissue and organ environments, as well as in studies of marine fouling.

Received 10th April 2025,
Accepted 24th July 2025

DOI: 10.1039/d5lc00349k

rsc.li/loc

Introduction

Microfluidics technology offers several advantages to life science research, such as reduced sample usage, high sensitivity and specificity, a high degree of functional integration, automation, the ability to probe unique biophysical phenomena, and the creation of unusual behaviors from cells, such as controlled mixing, bacterial conjugation, and mass transfer, to name only a few.[1–5] Microfluidic technology is a cornerstone of lab-on-a-chip (LOC) methodology, which offers countless advantages over traditional, bench-top methods. These advantages include miniaturization, automation, and enhanced high-throughput screening (HTS) abilities.[6–10] Additionally, microfluidic chips can be modular, meaning that the basic architecture of the chip can be placed on an arbitrary substrate of interest. This modularity enables rapid prototyping, customization, and adaptation to diverse applications.[11,12]

We applied a microfluidic approach to find a new way to screen biologically-inspired adhesives in high-throughput on an arbitrary polymer substrate. Certain polymers exhibit low surface energy and high hydrophobicity, rendering them relatively inert and difficult to functionalize or bond without using heat, or mechanical or chemical pre-treatment. In contrast, biological systems have developed sophisticated mechanisms to address a myriad of chemical challenges under Earth's diverse conditions, including the ability to adhere reversibly to challenging substrates and to adhere in wet environments.[13–15] Developing bioinspired, innovative strategies that facilitate strong adhesive bonding could enable on-site repairs of damaged plastic components and enable novel composites for applications such as enhanced capacitors. However, exploration of biologically-inspired adhesives is hampered by a paucity of high-throughput adhesive screening techniques. For instance, the technique of directed evolution, which has been used to produce substantial improvement in enzyme performance,[16,17] cannot

[a] United States Army Combat Capabilities Development Command (DEVCOM) Army Research Laboratory, USA. E-mail: jose.a.wippold.civ@army.mil
[b] University of Maryland, College Park, USA

currently be applied to solving adhesive problems without first developing appropriate high-throughput screening methods. Many adhesive-testing methods, such as lap shear, surface force analysis (SFA), or surface plasmon resonance (SPR), are low throughput and need substantial quantities of purified material, making it difficult to evaluate the vast array of possible adhesive proteins or peptides.

Initially, to solve this throughput problem, the Microfluidic Assessment of Adhesion of Peptides by Surface Display (MAPS-D) approach was developed as a semi-quantitative, on-cell, fluidics-based method to compare the ability of peptides to promote adhesion to substrates (separate publication forthcoming). Adhesive peptides were displayed on a bacterial surface, and the bacterial cells were allowed to adhere to a substrate of interest while being held within a commercial, single-channel microfluidic device. The cells were then subjected to a shear force in a microfluidic device. However, while MAPS-D did provide semi-quantitative binding information, we sought a higher-throughput solution. The present work demonstrates an improvement in this fluidics-based method for screening the adhesive interactions between peptides and proteins displayed on the surface of bacterial cells and polymethylmethacrylate (PMMA) or polycarbonate (PC) substrates (Fig. 1). The microfluidic platform presented here is the kappa(κ)Chip, or (κ)Chip, so named to reflect its ability to screen an in-house developed peptide library for binding. The kappa(κ)Chip method obviates the need to synthesize and purify individual peptides and requires no scale-up. The unique geometry of the device enables multiple shear rates to be evaluated with a single-input flow rate, enabling a 24-fold increase in the number of experiments that can be conducted compared to a commercially available chip. This work describes the design cycle, from conception through simulation to fabrication to testing and analysis, of the kappa(κ)Chip. The kappa(κ)Chip device improves the current state-of-the-art standard through a novel design approach, a less expensive and quicker fabrication method, and higher-throughput analysis, enabling more experiments to be run in less time. While existing microfluidic devices for cell adhesion screening have demonstrated broad utility, they often present limitations in experimental workflow and data quality.[18–21] While devices like those developed by Rupprecht *et al.* offer analytical capabilities, their multi-inlet designs increase experimental complexity.[22] Single-input devices, such as those by Ponmozhi *et al.*, suffer from reproducibility issues and utilize rudimentary components and procedures for device assembly.[23] Wei *et al.* demonstrated a novel approach to tackle high-throughput data acquisition using impedance analysis and automated data retrieval, but impedance analysis requires more technical skill and has not been proven to work at high resolution across many different

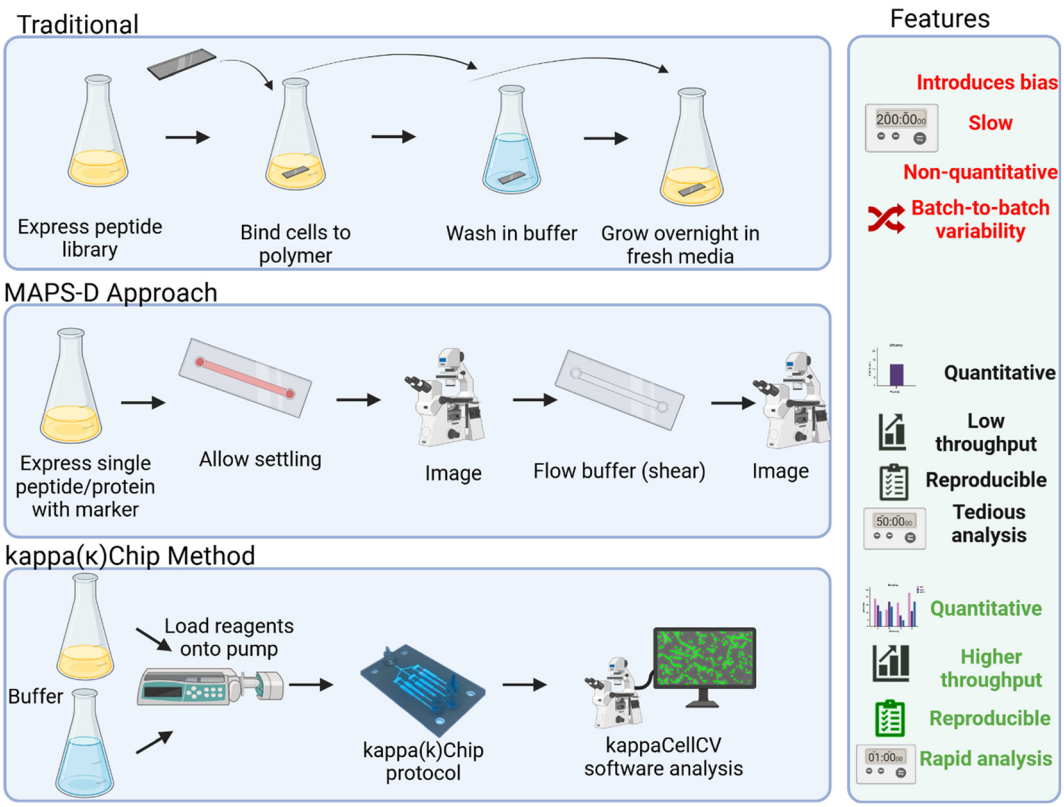

Fig. 1 Simplified workflow for kappa(κ)Chip compared to a traditional method and the MAPS-D (publication forthcoming) approach also developed by DEVCOM Army Research Laboratory. Benefits and features are demonstrated in the features sidebar. MAPS-D: Microfluidic Assessment of Adhesion by Surface Display (publication forthcoming).

organisms.[24] Critically, no current platform combines high-throughput data acquisition with a modular surface for versatile experimentation. Moreover, many existing devices rely on PDMS, a highly deformable material prone to channel distortion under pressure – a significant drawback for accurate cell adhesion studies. By etching the adhesive layer and assembling the device through this workflow, the problems of deformation are avoided.

To handle the large amount of data generated by the kappa(κ)Chip, we also developed image processing machine learning (ML) software (kappaCellCV), which is derived from OpenCV source code.[25] Image processing ML can play a crucial role not only in rapidly analyzing large volumes of data but also in correcting for shortcomings in the data, potentially caused by poor equipment or inexperienced operators. ML algorithms can accurately identify and analyze microscopic features, such as cells or particles, enabling precise measurements and insights. OpenCV is also free of experimenter-created bias when thresholding images, and has the potential to speed up research and development processes in fields that rely on microfluidic tools for support (drug discovery, high-throughput screening, biotechnology, and diagnostics, to name a few).

This pilot-screen work, consisting of proof-of-concept experiments, investigates a type of fungal protein called hydrophobins, which are generated by filamentous fungi and which have been studied for their adhesive properties.[26–29] Hydrophobins are displayed on the surface of cells using the well-characterized autotransporter display system derived from the EhaA adhesin protein of *E. coli*, which can display proteins larger than hydrophobins.[30,31] The cells also co-express green fluorescent protein (GFP) to enable them to be tracked, and fluorescent cells are subjected to shear stress in the kappa(κ)Chip. The retention of cells on a substrate of interest under shear stress serves as a direct measure of adhesion strength, which in turn reflects the extent to which the hydrophobin on the surface promotes adhesion. This provides an unbiased, rapid, and quantitative method to compare the expressed peptides of interest.

From a microfluidic manufacturing perspective, this work integrates multiphysics microfluidic device simulation in the design process, laser milling for cartridge fabrication, and ML for data processing (kappaCellCV). Laser milling enables the rapid fabrication of intricate microfluidic channels while providing precise control over channel geometry and dimensions, and is more versatile than competing microfabrication approaches, such as photolithography or chemical etching.[32]

Taken together, this work presents a complete workflow—from device conception to automated data analysis—for a microfluidic system that leverages a novel geometrical design, rapid fabrication and assembly, and high-throughput image analysis to overcome traditional barriers in peptide–substrate binding screening assays (Fig. 1). Our modular design allows for versatile integration with a variety of test substrates, as demonstrated through successful screening assays on both PMMA and PC. This flexibility is inherent to the fabrication and assembly methods developed, enabling straightforward adaptation to different materials and experimental needs without requiring redesign. This work introduces a powerful combination of parallelized assays and modular design, enabling rapid and customizable screening of analytes against diverse substrates. By providing the technical details found in this manuscript and practical know-how, we empower researchers to create tailored microfluidic solutions when commercial options are insufficient to address their specific needs. We anticipate that our microfluidic chip could be applicable to many types of analysis of adhesion under shear stress, such as cellular adhesion to substrates of interest, mammalian cellular adhesion in an organ or organoid-type setting, or analysis of marine fouling.

Methods

Device design

For all microfluidic chip channel configurations tested in the manuscript, the consumables (*i.e.* microfluidic test chips) were designed initially using AutoCAD (Autodesk Inc. Boston, MA). Following design completion, the files were saved as .dwg file types and imported into CorelDRAW (Alludo, Ottawa, Canada) to generate laser-ablation–compatible layer files.

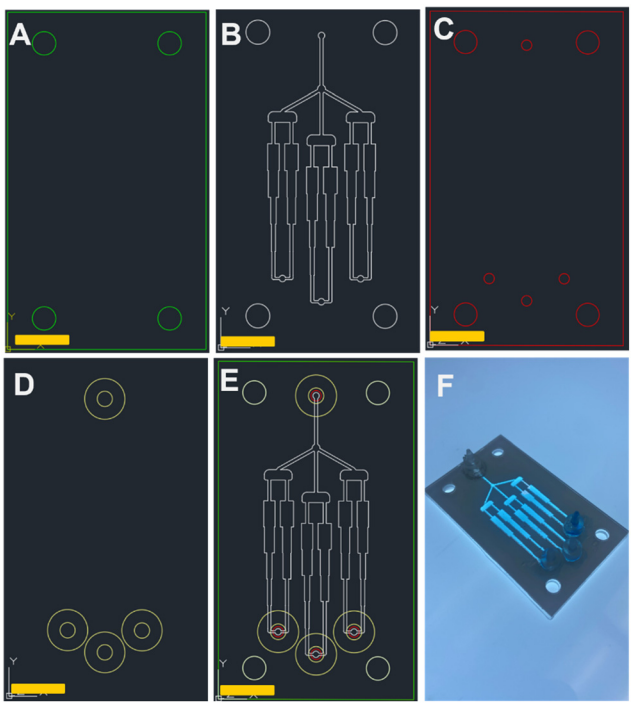

Fig. 2 Kappa(κ)Chip layer schematics. A. Bottom substrate for hydrophobin–polymer interaction tests. B. Adhesive/channel layer to define internal shear stresses. Three identical units containing eight shear stress tests. C. Top cover (PMMA) design. D. Double-sided adhesives for connecting microfluidic interfacing parts. E. Combined schematic of all layers. F. Fully assembled kappa(κ)Chip. Yellow scale bar is 10 mm.

The kappa(κ)Chip is constructed from five layers (Fig. 2A–E, from bottom to top). For layer 1, or the bottom-most layer, a 38.1 × 64.9 mm rectangle of the material of interest was cut using a CO_2 laser cutting tool. Four 4 × 4.5 mm diameter circles were cut in this rectangle, and these circles were used as registration and alignment marks to ensure layer-to-layer alignment during the assembly process. Layer 2 consisted of the microfluidic channels built out of a double-sided pressure-sensitive adhesive (PSA) (ARCare 8939, Adhesives Research, Glen Rock, PA). Pressure-sensitive adhesives (PSAs) are a critical and widely used, yet often unseen, component in the manufacturing of both high-volume and point-of-care diagnostic and microfluidic devices.[34,35] Their ease of use, low cost, and reliable bonding capabilities make them essential for major manufacturers across the commercial landscape.[36–38] Layer 2 defines the geometry of the microfluidic assembly design (Fig. 2B, SI S2A). Layer 2 has three "branches" (BI, BII, BIII) serving as on-chip technical replicates (SI Fig. S2A). SI Fig. S2A provides a schematic of the branches and zones for the developed microfluidic platform. Each branch consists of a channel, which becomes narrower as the fluid flow proceeds. The wide-to-narrow tapering of channels increases local velocity under the assumption of a constant injection rate, and this results in eight distinct shear zones on the same chip. The height of layer 2 (channel layer) was set to 126 μm and maintained uniformly across all zones.

Layer 3 consisted of a PMMA rectangle (again 38.1 × 64.9 mm with 4 × 4.5 mm diameter circles for alignment) with four additional through-holes (2 mm diameter) used as fluidic communication ports (one inlet, three outlets). Above layer 3, layer 4 consists of four doughnut-shaped double-sided PSA connectors (outer diameter 8 mm; inner diameter 3 mm) used to attach custom 3-D printed barb connectors (layer 5). These barb connectors allowed for 1/16″ tubing to communicate between the sample and the chip.

Device fabrication and consumable assembly

Device fabrication

Microfluidic chips were fabricated using a combination of laser ablation and 3D printing. PMMA and polycarbonate substrates were laser-cut to create the base and cover layers, which were then bonded together using a pressure-sensitive adhesive (PSA; refer to supplementary information for details). Laser ablation was used to etch the channel geometry into the PSA-laden substrates, followed by a pre-assembly quality-controlled preparation method to ensure the layers were suitable for experimentation (refer to supplementary information for details). 3D-printed barb connectors were used for fluidic interfacing. Precise alignment was ensured by assembling the layers using a 3D-printed alignment rig. The current batch workflow yields six fully assembled devices in 3 h (two devices per hour). This timeframe includes processing from commercial off-the-shelf components through fabrication and assembly. This could be further reduced upon optimization of production.

Device characterization methods

Microfluidic flow simulations

COMSOL Multiphysics 6.1 (COMSOL, Inc. Burlington, MA) was used to run multiphysics flow simulations on the designed channel systems. The designs were copied from AutoCAD and imported into SolidWorks to enable a 3-dimensional positive-feature structuring of the fluidic geometry system. The CAD models were then imported into the COMSOL interface using the Geometry import module. For all simulations, the temperature was set to 293.15 K and the material properties of water were assigned. We assigned Laminar flow (spf) physics interface parameters to indicate the fluid properties and initial values of wall, inlet, and outlets. Fluid properties were set to a common model input for temperature, a density (ρ) value of 1000 kg m^{-3}, and a dynamic viscosity (μ) of 1.0 × 10^{-3} Pa × s. All initial values were set to zero and a wall condition of No Slip was assigned. Additionally, a fully developed flow was assigned at an average velocity (U_{av}) of 0.00201154 m s^{-1}. For the outlet conditions, the pressure was set to static at a value of 101 325 Pa. For finite element analysis, a physics-controlled mesh with an element size selection of Normal was used to balance reliable simulations with computing intensity.

Pilot screen

To test the developed microfluidic screening capabilities, a pilot screen was developed using a previously prepared surface display library expressing hydrophobins which are displayed on the surface of *E. coli*.[33] Two example hydrophobins from the library were used as test samples for this sample screen. The class I hydrophobin EAS, derived from the fungus *Neurospora crassa*, was designated AT12 (UniProt accession number Q04571) and the hydrophobin DewA, derived from the fungus *Aspergillus nidulans*, was designated AT13 (UniProt accession number P52750). The sequences used were derived from the UniProt database and codon-optimized for *E. coli* using IDT's Codon Optimization Tool. Additionally, the control strain which contained Intermediate 2 rather than a full construct, termed ATEmpty, was employed as a negative control, as this sample should not have any "sticky" protein or peptide expressed on its surface. In addition to this control, another set of controls was employed by running uninduced states (where the "sticky" protein is presumably not displayed) of both AT12 and AT13 samples. The kappa(κ)-chip modular system was used to screen these samples against two preliminary substrates of interest, PC and PMMA, to elucidate peptide binding tendencies (Fig. 3).

For pilot-screen experiments, a fresh colony from the agar plate was selected and cultured overnight. AT12 and AT13 strains were cultured in 5 mL of LB liquid broth containing 30 μg mL^{-1} and 100 μg mL^{-1} of chloramphenicol and

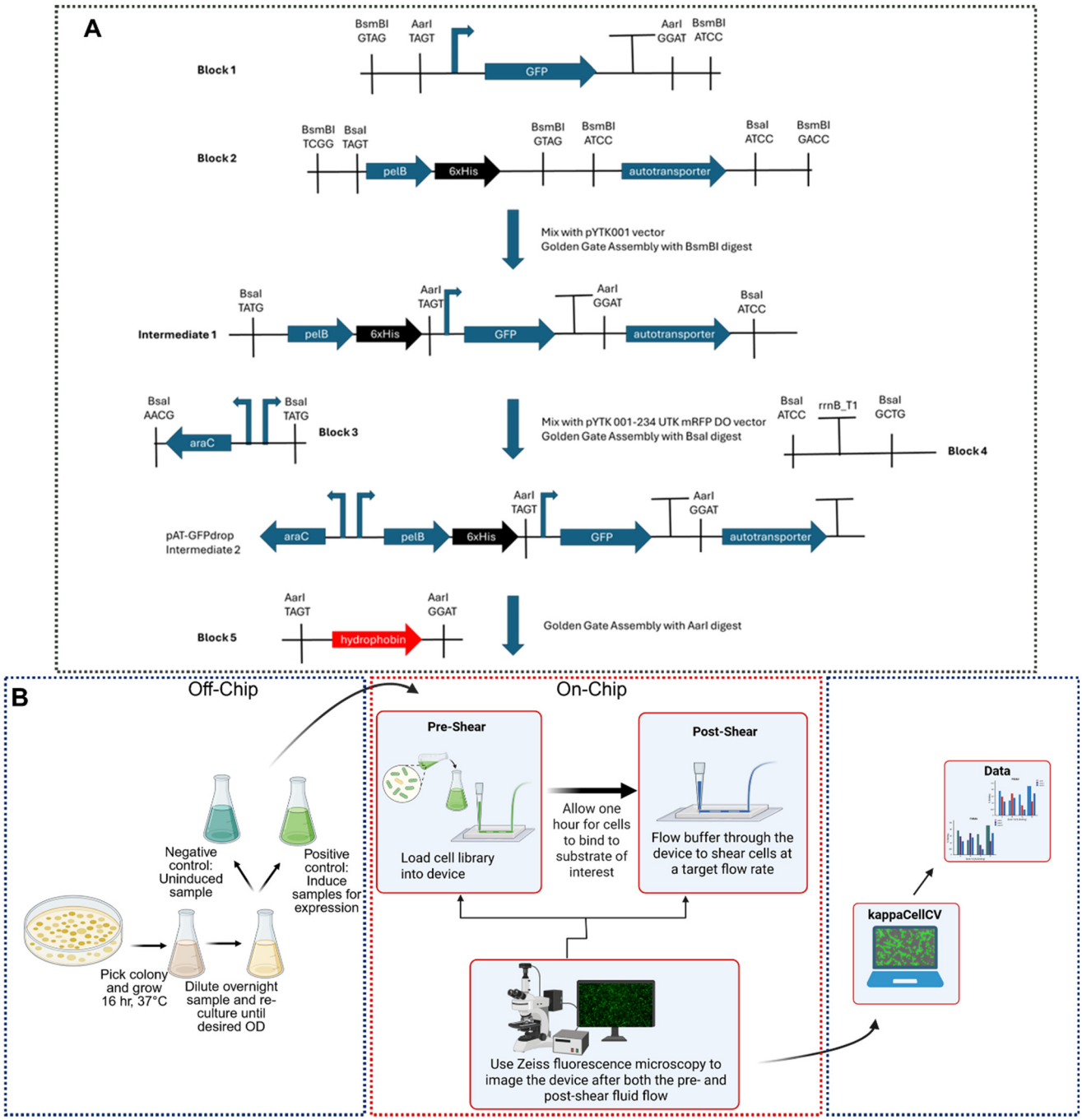

Fig. 3 Kappa(κ)Chip pilot screen workflow. A. Cloning strategy to obtain hydrophobin surface display construct. B. Schematic workflow for the kappa(κ)Chip employed in this work.

ampicillin, respectively. ATEmpty samples were cultured in pure LB broth in a shaking incubator set to 37 °C and 225 rpm. Following overnight culture, 75 μL of the overnight culture was diluted into a fresh 5 mL of their preferred medium and returned to the shaking incubator under the same conditions for 2 h. For induced samples, 50 μL of 10% w/v L-arabinose was added to induce hydrophobin expression, and the samples were returned to the incubator for another 1 h. For uninduced samples, the culture tubes were left undisturbed for 3 h. After the culture period, the expected OD600 for the samples would range from 0.15 to 0.30. Prior to experimentation, the samples were filtered through a 10 μL cell strainer (VWR MSPP-435001003) and then adjusted to 0.15 OD for the desired assay seeding density. The cells were then loaded into a 5 mL syringe (BD, VWR) and a polypropylene luer-lock barb connector was fitted onto the syringe (45508-00, VWR). In a separate 10 mL syringe, 0.02% w/v Tween 20 in PBS flow buffer was loaded and again fitted with a polypropylene luer-lock barb connector, to be used as the shear buffer solution. The syringe was connected to

Tygon® tubing (Saint-Gobain, Courbevoie, France). Both fluidic communication lines were connected to a 4-way stopcock luer (14057-10 World Precision Instruments, Sarasota, FL) that fed into a single output tubing line. After priming all the tubing lines to prevent trapping of air bubbles, the single output line was connected to the kappa(κ) Chip test chip. Both syringes were loaded onto syringe pumps (Fusion 200X, Chemyx, Sugarland, TX) for precise sample injection. After adjusting the valve to prevent backflow into the buffer line, the cell sample was set to inject at a flow rate of 5000 μL h^{-1} for 5 min. Following this flow period, cells were allowed to seed for 45 min before the device was placed in a custom 3D-printed adapter for use on a Zeiss Colibri microscope stage for image acquisition (see section on Image Acquisition and Microscopy for additional details). After one hour of seeding, the stopcock valve was adjusted to prevent backflow into the cell sample line, and the buffer line was set to 8190 μL h^{-1} for 10 min to induce variable range of shear stress within the microfluidic system. Following this flow, the kappa(κ)Chip was again imaged to obtain post-flow data. This pilot-screen experiment was repeated using an 81 900 μL h^{-1} injection flow rate on a PMMA substrate to clarify any shear force phenomena present on the protein-expressed cells in the various zones of the microfluidic device.

Image acquisition and microscopy

For all experiments, experimental images were captured using an inverted Zeiss Colibri Axio Observer microscope (Carl Zeiss Microscopy, LLC. White Plains, NY) fitted with a temperature and humidity enclosure around the automated stage. For data acquisition, a customized program from image acquisition was established within Zen Pro to ensure images at the same coordinates for pre-shear and post-shear data time points. For all brightfield images, 9 V light illumination was used with a Ph1 (0.55NA) and 10× objective, applying a T400lp paired with an analytical DIC transmission light filter at 14 ms exposure. For all fluorescent images, a 475 nm LED (100% power) was used with a 10× objective applying a T495lpxr beamsplitter with a BP 520/50 emission filter at 750 ms exposure.

kappaCellCV

Computer-vision-enabled cell-counting software was developed using the OpenCV module in Python for high-speed image analysis. The software converts a 200 × 200-pixel2 sample of a brightfield microscopy image to grayscale and applies an adaptive Gaussian threshold (AGT), returning a binary image highlighting cell contours. To apply AGT, the user selects a suitable noise reduction value and a 'pixel neighborhood' size based on a preliminary sample image from the dataset. By determining a normalized contrast threshold for each pixel neighborhood across the image, AGT excludes incidental lighting abnormalities and irregularities in each image, compared to industry-standard image-based automated cell-counting software. The number of complete contours is then counted and highlighted by the software. The software was validated against manual cell counting with less than 3% error in image count triplicate (*e.g.* recounting the same image three times) for three different image tests under each test condition. kappaCellCV processes each image in a designated folder and outputs raw data in the form of an .xlsx file with user-inputted column identifiers to distinguish each image. These identifiers are used in the naming convention, which the user is responsible for upholding when creating image sets.

Results

Device fabrication and consumable assembly

The microfluidic chips were assessed to determine the accuracy and precision of the chosen fabrication methods. These results were obtained by measuring, in triplicate, the channel widths of each zone (1–8) on each branch (technical replicates housed on the chip) for three consecutive devices, totaling 216 individual measurements using an optical profilometer (Keyence VHX700 Itasca, IL). The results showed a consistent fabrication method with maximum standard deviation observed at 15 μm from the intended width and all under 1% percent error when compared to the CAD design for the channel layer (see SI Fig. S2 and S3). Additionally, the three branches (designated 1–3 from left to right, see SI Fig. S2A) demonstrated consistent widths between all assessed trials.

The consumables were assembled using a heat press to standardize the channel thickness layer during fabrication. The average thicknesses for 5 MPa/1 min and 5 MPa/5 min conditions were 173 μm and 149 μm, respectively (see SI Fig. S4). The average thicknesses for 10 MPa/1 min and 10 MPa/5 min conditions were 151 μm and 126 μm, respectively (see SI Fig. S4).

Flow simulations and image analysis

Through an iterative design process encompassing 20 variations, we observed that the theoretical velocity predictions for isolated channel geometries deviated from full-device simulation results in the initial designs. Only through repeated iterations of the design, were we able to ensure a strong correlation between channel width and flow rate. The final design of the chip (SI Fig. S2) is somewhat counterintuitive. The widest part of the channel is designated as zone 1, and the narrowest part of the channel is designated as zone 8. The zones are arranged in a ladder-like pattern, with the right-hand side of the stem having zones 1, 4, 5 and 8 and the left-hand part of the stem having zones 2, 3, 6, and 7, as shown. This highlights the importance of whole-device simulation in our optimization strategy. Microfluidic flow simulations were used to elucidate the fluidic dynamics of the channels (Fig. 4, SI S5). Through data extraction from the COMSOL models, the velocity magnitudes for the 1× rate experiments were 0.0015 m s^{-1},

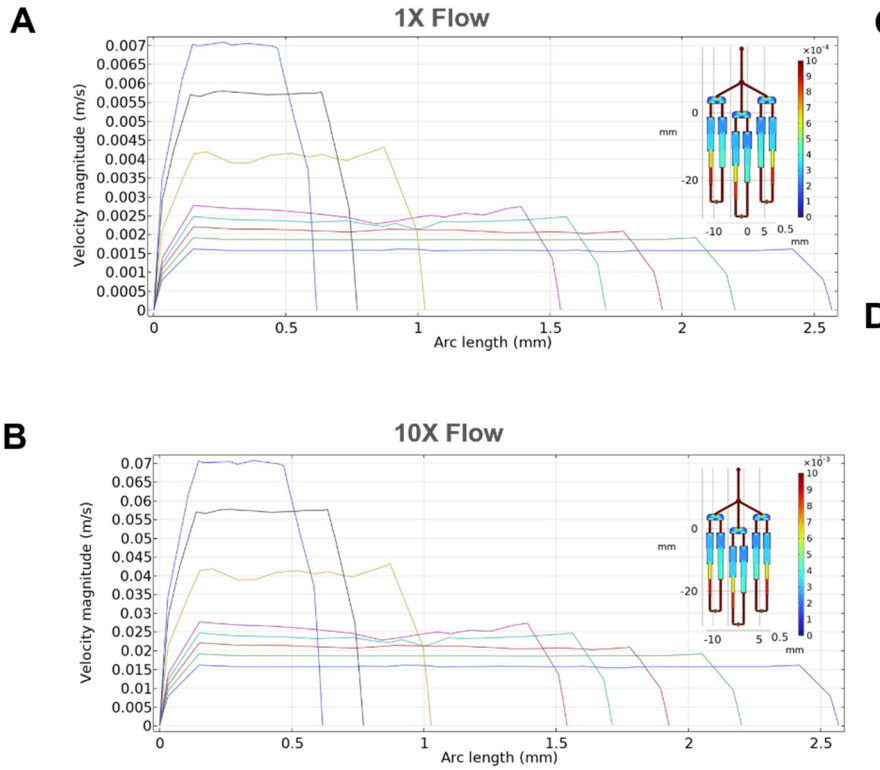

Velocity Magnitudes		
	1X (x 10^{-3} m/s)	10X (x 10^{-3} m/s)
Zone 1	1.50	15.00
Zone 2	1.90	17.5
Zone 3	2.12	20.00
Zone 4	2.60	22.50
Zone 5	2.75	25.00
Zone 6	4.00	40.00
Zone 7	5.60	57.50
Zone 8	7.00	70.00

Fig. 4 COMSOL simulation results demonstrating decreases in velocity magnitude as channel width increases. A. 1× Flow pattern using the final kappa(κ)Chip version. B. 10× Flow pattern using the final kappa(κ)Chip version. C. Arc length visual representation. Arc length in yellow. D. Velocity magnitudes extracted from A and B.

0.001900 m s^{-1}, 0.00212 m s^{-1}, 0.00260 m s^{-1}, 0.00275 m s^{-1}, 0.00400 m s^{-1}, 0.0056 m s^{-1}, and 0.007 m s^{-1} for zones 1–8, respectively. Correspondingly, these flow rates resulted in actual shear stresses of 0.643 dyne cm^{-2}, 0.814 dyne cm^{-2}, 0.911 dyne cm^{-2}, 1.114 dyne cm^{-2}, 1.178 dyne cm^{-2}, 1.714 dyne cm^{-2}, 2.400 dyne cm^{-2}, and 3.00 dyne cm^{-2} for zones 1–8, respectively. For Fig. 4, the arc length represents the length of the line used to obtain the velocity magnitude data points. Specifically, it corresponds to the distance from one channel wall to the other in a straight line perpendicular to the flow direction.

For the 10× rate experiments, the velocity magnitudes of flow were 0.0150 m s^{-1}, 0.0175 m s^{-1}, 0.0200 m s^{-1}, 0.0225 m s^{-1}, 0.0250 m s^{-1}, 0.0400 m s^{-1}, 0.0575 m s^{-1}, and 0.0700 m s^{-1} for zones 1–8, respectively. Correspondingly, these flow rates resulted in actual shear stresses of 6.430 dyne cm^{-2}, 7.500 dyne cm^{-2}, 8.571 dyne cm^{-2}, 9.643 dyne cm^{-2}, 10.71 dyne cm^{-2}, 17.14 dyne cm^{-2}, 24.64 dyne cm^{-2}, and 30.00 dyne cm^{-2} for zones 1–8, respectively. Shear stress forces were also compared to potential drag forces in the microfluidic channels (see supplementary methods for calculations; see SI Fig. S6 for data). Shear forces were assumed in a regime where the flow is into the "face" of a cell and also into the body of a cell. Shear forces ranged from 50.49 fN to 600 fN for 1× flow experiments and from 504.9 fN to 6000 fN for the 10× flow experiments. Drag forces were assumed in a regime where the flow is into the "face" of a cell and also where the flow is into the body a cell. Drag forces ranged from 1.060 fN to 58.60 fN for the 1× flow experiments and from 106.0 fN to 5880 fN for the 10× flow experiments. These results indicated that the governing physical phenomena for shear experiments were indeed the shear forces resulting from the shear flow.

Experimental images obtained during the shear experiments were batch analyzed using the kappaCellCV program scripted for this study (SI Fig. S7). In brief, the program counted the cells in image folders with over a 1000× reduction in time compared to manual counting (4 s per experiment *vs.* 4 h for manually counting and registering 96 images). Images were either selected to be analyzed in full-frame mode or in cropped mode, depending on the presence of undesirable artifacts during fabrication (SI Fig. S8).

Pilot screens

Both PMMA and PC substrates were chosen as potential materials of interest and subjected to workflow testing. For both substrates of interest, two proteins of interest (hydrophobins DewA and EAS) that were down-selected in previous efforts (data not shown) were used on the *E. coli* system. For all experiments, both the induced (presumably peptide expressing) and uninduced (no peptide) samples were screened for binding efficiency along with an additional control, the ATEmpty construct (which expressed no

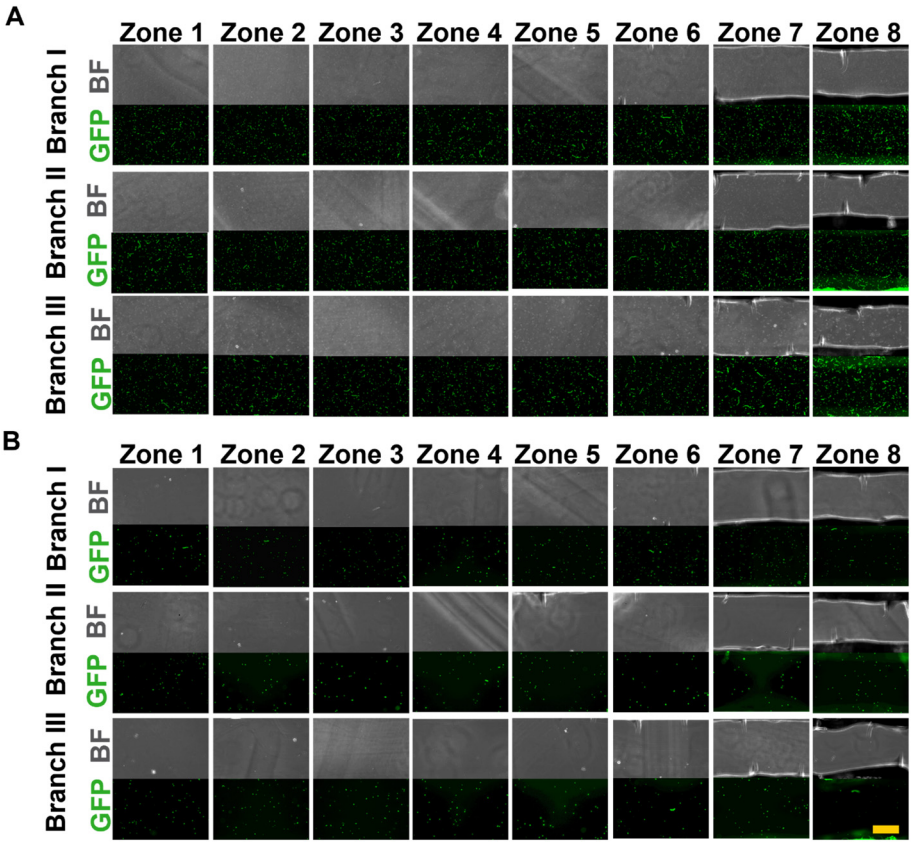

Fig. 5 Experimental micrographs obtained from a representative kappa(κ)Chip experiment from both pre-shear (A) and post-shear (B) time points. Each zone represents a separate flow experiment and data point. The dataset would then be analyzed with the kappaCellCV software for image processing and data quantification. Yellow scale bar is 100 μm.

recombinant protein or peptide on the surface), to account for any baseline adhesion of the chassis *E. coli*. Microscopy images were captured (Fig. 5) and recorded for downstream data processing through the kappaCellCV software.

A significant difference in adhesion was observed in all zones of the PMMA samples (1–8) when comparing induced against uninduced samples (Fig. 6A). Both induced AT12 and AT13 demonstrated comparable adhesion in all zones. Interestingly, the AT12 induced population had the tightest data distribution, indicating the unique suitability of the kappa(κ)Chip system. For the PC substrate (Fig. 6B), a similar overall trend was observed, in that the induced samples, both AT12 and AT13, showed significant differences when compared to their respective uninduced controls along with the ATEmpty chassis control. After amending the screening approach by increasing the flow rate tenfold, from 8190 μL h^{-1} to 81 900 μL h^{-1}, it was found that there were clear differences between AT12 and AT13 and their respective controls. It was further found that there was a clear difference in the number of cells that were retained in each zone, with higher nominal shear rates in a zone correlating to fewer cells remaining. This demonstrated the ability of the kappa(κ)Chip to identify and differentiate promising peptides at different shear force intervals (Fig. 6C). We observed substantial adhesion in the uninduced AT12 and AT13 samples, likely from leaky expression of the hydrophobin constructs. Despite this, the induced samples still adhered significantly more than the uninduced ones on both substrates. However, the ATEmpty construct, which has no hydrophobin present and whose autotransporter gene is out of frame with the arabinose promoter, is a bare *E. coli* cell: it does not have any adhesive protein to express. In the ATEmpty controls, observed cellular adhesion is much less, demonstrating that shear forces effectively remove non-adherent cells and confirming the ability of this method to distinguish adhesive from non-adhesive cells. The kappa(κ)Chip generates a rigorous amount of data during experimentation. In Fig. 6A–C, one star indicates a p-value $<$ 0.05, two stars indicate a p-value $<$ 0.01, three stars indicate a p-value $<$ 0.001, and four stars indicate a p-value $<$ 0.0001. For the 1× flow testing (Fig. 6A and B), every induced sample (AT12 and AT13) displayed a significant difference from the true negative control (ATEmpty). However, four induced conditions in the 1× PMMA (Fig. 6A) regime displayed a statistically significant binding difference (AT13 zone 1 and AT13 zone 8; AT13 zone 2 and AT13 zone 8; AT12 zone 1 and AT12 zone 8; AT12 zone 2 and AT12 zone 8). Two conditions in the 1× PC (Fig. 6B) regime displayed a statistically significant binding difference (AT13 zone 1 and AT13 zone 8; AT13 zone 2 and AT13 zone 8). Fig. 6C presents the

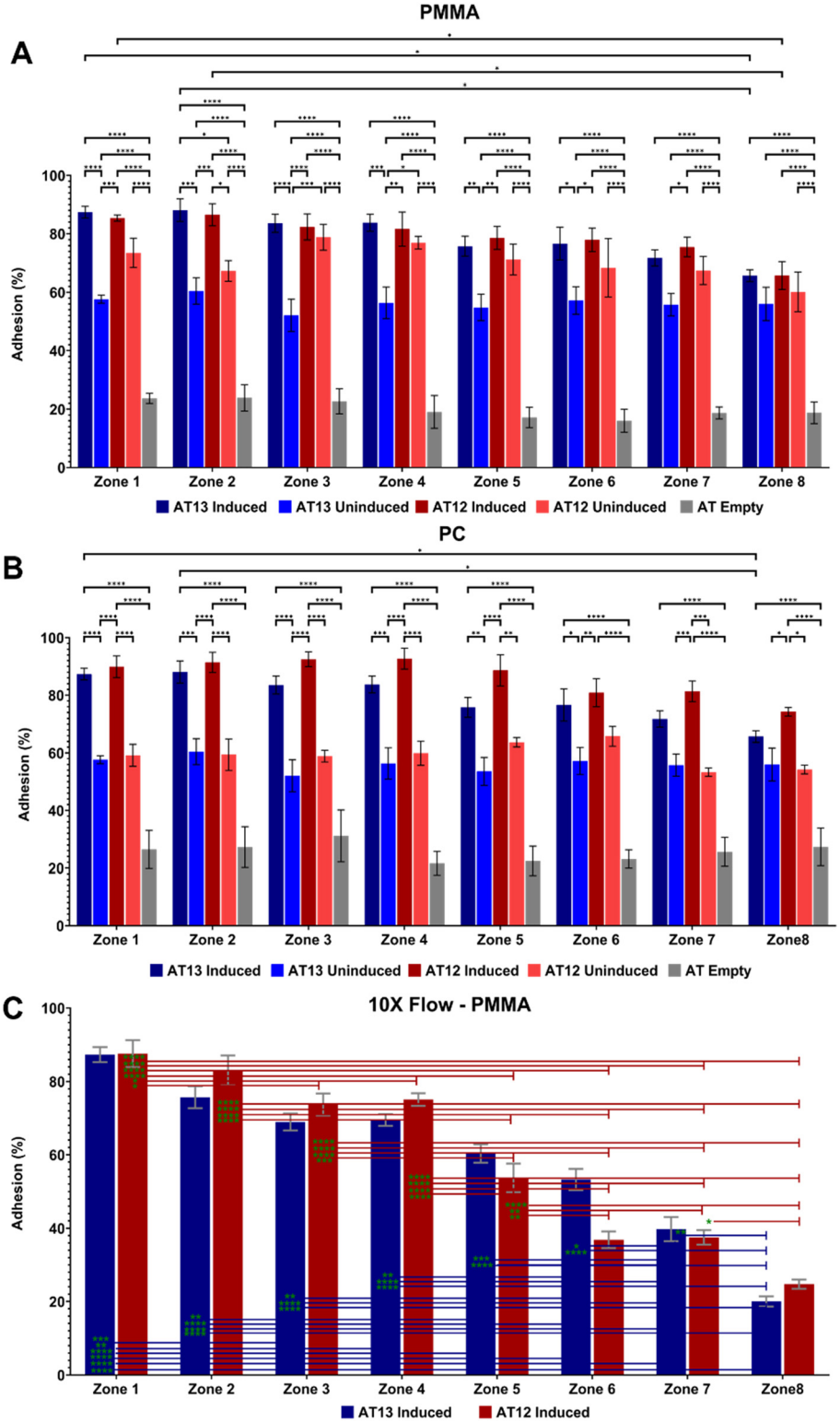

Fig. 6 Pilot screen adhesion results. A. 1× Flow on PMMA. B. 1× Flow on PC. C. 10× Flow on PMMA. Error bars denote standard error of mean (SEM). One star indicates $p < 0.05$, two stars indicate $p < 0.01$, three stars $p < 0.001$, four stars $p < 0.0001$.

traditional bracket under asterisk data as green stars (replacing the black asterisks), with color-coded bars (replacing the brackets) to present the data in a more reader-friendly manner. For the 10× flow regime on PMMA (Fig. 6C), both AT13 induced and AT12 induced conditions displayed statistically significant binding differences. It should be noted that no like-for-like tested sequence (*i.e.* AT 13 to AT13 or AT12 to AT12) displayed differences to the zone closest to

it (*e.g.* zone 1 to zone 2, zone 2 to zone 3, etc). However, this paradigm changes for conditions in zones 5–8, where all tested conditions were statistically different from the zones closest to it, except in the case of AT12 induced zone 6. Intuitively, this paradigm change is not surprising, given that the internal velocity magnitudes of zones 1–4 increase in smaller steps compared to zones 5–8 (see COMSOL data in Fig. 4A and B).

Conclusion

By leveraging microfluidics, researchers can accelerate their studies, increase efficiency and experimental throughput, and gain deeper insights into complex biological systems. Microfluidic technology is particularly attractive to the biological sciences because biological samples are often scarce and produced on a small scale, and the compositional space and number of variables in which biologists operate are very large. In this work, a microfluidic device was created to help search for a biological solution to a pressing problem in materials science: that of developing strong adhesive bonds between polymers and other surfaces. Biological systems have evolved sophisticated mechanisms to adhere to diverse surfaces, even in wet environments. The world of biology might therefore provide novel ways of solving adhesive problems, but finding the correct potential adhesive in a large compositional space is challenging, as most adhesive assays are low throughput, or require relatively large amounts of material, or both.

In this work, a novel microfluidic platform, the kappa(κ) Chip, has been developed to screen the adhesive interactions between proteins and polymers in higher throughput while requiring less material. This device enables researchers to rapidly test and identify strong adhesive proteins, which could be used to develop novel adhesives, coatings, and composites. The kappa(κ)Chip offers a 24-fold increase in experimental throughput compared to commercial microfluidic methods, making it an attractive tool for researchers seeking to accelerate their studies. Our work also presents a comprehensive overview of the process required to resolve a shortcoming in the commercial arena, and suggests a novel method of making microfluidic devices; rather than directly ablating PMMA, we utilized laser ablation to precisely pattern pressure-sensitive adhesive (PSA). This created microfluidic channels with smooth top and bottom surfaces ideal for our binding assay, while still leveraging the rigidity and optical clarity of PMMA for robust shear experiments and real-time cell observation in a low-cost, scalable device.

Our work also provides an important reminder that flow simulations do not scale linearly (*i.e.* results for a 10× injection rate do not scale to the 1× injection rate by a factor of ten), and that whole-device simulations are necessary to obtain accurate results, which is important to consider within the context of microfluidic product development. Analyzing microfluidic devices by isolating components and modelling them individually often yields oversimplified results that fail to accurately predict overall system performance. As the field progresses towards translational development, a more holistic approach, such as the one adopted here—one that recognizes the complex interconnectedness of the entire device geometry—is essential for accurate analysis and successful design.

There are three limitations to the kappa(κ)Chip: first, the channel height is relatively large compared to the size of bacterial cells (~150 μm channel *vs.* ~2 μm cell), meaning that the flow faced by the cells is likely to be subject to edge effects and lower than the nominal flow calculated: this explains the need to increase the flow rate by 10× to see clear differentiation in adhesion between zones. Second, to further increase the device throughput, more channels are required and therefore decreased channel widths are needed to maintain the same "business-card" footprint. While laser milling is known to be precise over a minimum feature-size threshold, laser milling would not be an appropriate microfabrication technique to increase the throughput of a kappa(κ)Chip by an order of magnitude (*i.e.* 10× the number of channels necessitating a 10× feature size reduction). Third, the kappaCellCV software is currently limited to the analysis of transparent substrates and struggles on opaque substrates, such as high-density polyethylene (HDPE) or polypropylene (PP). However, despite these limitations, by combining microfluidics, microfabrication, and machine learning data analysis, the kappa(κ)Chip provides a powerful platform for exploring the complex interactions between biological systems and synthetic materials, with potential applications in fields such as biomedical engineering, materials science, and environmental science.

Author contributions

J. A. W. contributed to the conceptualization, data curation, formal analysis, investigation, methodology, project administration, resources, software, supervision, validation, visualization, writing – original draft, and writing – review & editing. M. T. K. contributed to the conceptualization, data curation, investigation, methodology, writing – original draft, and writing – review & editing. J. L. F. contributed to the methodology, software, and writing – original draft. J. B. contributed to the investigation and methodology. A. G. contributed to the investigation and methodology. J. P. J. contributed to the conceptualization, resources, and project administration. J. A. O. contributed to the conceptualization, resources, and project administration.

Conflicts of interest

Various contributing authors have filed a patent application pertaining to the scientific merit disclosed in this work. The authors believe this patent application does not compromise the objectivity of the presented research.

Data availability

Supplementary information is available: Additional fabrication data, quality assurance data, and simulation data can be found in the supplementary data linked here. See DOI: **https://doi.org/10.1039/D5LC00349K**.

Data reported in this manuscript are presented graphically in the figures contained within the main text and within the supplementary information. Additional data dispositions which form the foundations of this paper will be shared by the lead contact author upon request.

Acknowledgements

The authors would like to thank the Transformational Synbio for Military Environments (TRANSFORME) program. This project was also supported in part by the Office of the Under Secretary of Defense's SEED Early Career grant (J. Wippold). Additionally, the National Security Scholars Summer Internship Program (NSSSIP) supported the work as part of the Data Driven Engineering Research (DataDrivER) Cooperative Agreement between DEVCOM ARL and University of Maryland, College Park (J. La Fiandra, J. Boetticher, A. Grafton).

References

1 J. A. Wippold, M. Chu, R. Renberg, Y. Li, B. Adams and A. Han, *New Biotechnol.*, 2024, **81**, 10–19.
2 C. Huang, J. A. Wippold, D. Stratis-Cullum and A. Han, *Biomed. Microdevices*, 2020, **22**, 76.
3 H. Zhang, A. R. Guzman, J. A. Wippold, Y. Li, J. Dai, C. Huang and A. Han, *Lab Chip*, 2020, **20**, 3948–3959.
4 J. A. Wippold, H. Wang, J. Tingling, J. L. Leibowitz, P. de Figueiredo and A. Han, *Lab Chip*, 2020, **20**, 1628–1638.
5 J. Q. Boedicker, M. E. Vincent and R. F. Ismagilov, *Angew. Chem., Int. Ed.*, 2009, **48**, 5908–5911.
6 H. Huang and D. Densmore, *Lab Chip*, 2014, **14**, 3459–3474.
7 D. Gao, F. Jin, M. Zhou and Y. Jiang, *Analyst*, 2019, **144**, 766–781.
8 N. Convery and N. Gadegaard, *Micro Nano Eng.*, 2019, **2**, 76–91.
9 P. C. Gach, K. Iwai, P. W. Kim, N. J. Hillson and A. K. Singh, *Lab Chip*, 2017, **17**, 3388–3400.
10 M. K. Alam, E. Koomson, H. Zou, C. Yi, C.-W. Li, T. Xu and M. Yang, *Anal. Chim. Acta*, 2018, **1044**, 29–65.
11 X. Lai, M. Yang, H. Wu and D. Li, *Micromachines*, 2022, **13**(8), 1363.
12 J. Wu, H. Fang, J. Zhang and S. Yan, *J. Nanobiotechnol.*, 2023, **21**, 85.
13 W. Wang, Y. Liu and Z. Xie, *J. Bionic Eng.*, 2021, **18**, 1011–1044.
14 Y. Li and Y. Cao, *Nanoscale Adv.*, 2019, **1**, 4246–4257.
15 J. H. Waite, *J. Exp. Biol.*, 2017, **220**, 517–530.
16 S. Basler, S. Studer, Y. Zou, T. Mori, Y. Ota, A. Camus, H. A. Bunzel, R. C. Helgeson, K. N. Houk, G. Jiménez-Osés and D. Hilvert, *Nat. Chem.*, 2021, **13**, 231–235.
17 Y. Wang, P. Xue, M. Cao, T. Yu, S. T. Lane and H. Zhao, *Chem. Rev.*, 2021, **121**, 12384–12444.
18 E. Décavé, D. Garrivier, Y. Bréchet, B. Fourcade and F. Bruckert, *Biophys. J.*, 2002, **82**, 2383–2395.
19 Z. Tang, Y. Akiyama, K. Itoga, J. Kobayashi, M. Yamato and T. Okano, *Biomaterials*, 2012, **33**, 7405–7411.
20 H. Lu, L. Y. Koo, W. M. Wang, D. A. Lauffenburger, L. G. Griffith and K. F. Jensen, *Anal. Chem.*, 2004, **76**, 5257–5264.
21 K. V. Christ, K. B. Williamson, K. S. Masters and K. T. Turner, *Biomed. Microdevices*, 2010, **12**, 443–455.
22 P. Rupprecht, L. Golé, J. P. Rieu, C. Vézy, R. Ferrigno, H. C. Mertani and C. Rivière, *Biomicrofluidics*, 2012, **6**, 14107–1410712.
23 J. Ponmozhi, J. M. R. Moreira, F. J. Mergulhão, J. B. L. M. Campos and J. M. Miranda, *Micromachines*, 2019, **10**(5), 303.
24 M. Wei, R. Zhang, F. Zhang, Y. Zhang, G. Li, R. Miao and S. Shao, *ACS Sens.*, 2019, **4**, 2654–2661.
25 C. Domínguez, J. Heras and V. Pascual, *Comput. Biol. Med.*, 2017, **84**, 189–194.
26 I. Sorrentino, M. Gargano, A. Ricciardelli, E. Parrilli, C. Buonocore, D. de Pascale, P. Giardina and A. Piscitelli, *Int. J. Biol. Macromol.*, 2020, **164**, 2293–2300.
27 J. Q. Boedicker, M. E. Vincent and R. F. Ismagilov, *Angew. Chem., Int. Ed.*, 2009, **48**(32), 5908–5911.
28 M. Khalesi, K. Gebruers and G. Derdelinckx, *Protein J.*, 2015, **34**, 243–255.
29 F. Zampieri, H. A. B. Wösten and K. Scholtmeijer, *Materials*, 2010, **3**, 4607–4625.
30 E. Marín, G. Bodelón and L. Fernández, *J. Bacteriol.*, 2010, **192**, 5588–5602.
31 T. J. Wells, O. Sherlock, L. Rivas, A. Mahajan, S. A. Beatson, M. Torpdahl, R. I. Webb, L. P. Allsopp, K. S. Gobius, D. L. Gally and M. A. Schembri, *Environ. Microbiol.*, 2008, **10**, 589–604.
32 E. Sollier, C. Murray, P. Maoddi and D. Di Carlo, *Lab Chip*, 2011, **11**, 3752–3765.
33 M. T. H. Kozlowski, R. A. Hughes, R. M. Pullen and J. A. Orlicki, *Peptide and Hydrophobin Interactions with Polymeric Substrates Screened by a Bacterial Surface Display Method*, DEVCOM Army Research Laboratory, 2021, **https://apps.dtic.mil/sti/citations/AD1150281**.
34 C. A. Barrios, *Sensors*, 2020, **20**(18), DOI: **10.3390/s20185303**.
35 U. Abbasi, P. Chowdhury, S. Subramaniam, P. Jain, N. Muthe, F. Sheikh, S. Banerjee and V. Kumaran, *Sci. Rep.*, 2019, **9**, 18583.
36 S. Smith, M. Sypabekova and S. Kim, *Biosensors*, 2024, **14**, 249.
37 J. Jeon, J. Kim, S. Park, G. Bryan, T. J. Broderick, M. Stone and V. V. Tsukruk, *ACS Appl. Mater. Interfaces*, 2024, **16**, 48257–48268.
38 P. Ossowicz-Rupniewska, P. Bednarczyk, M. Nowak, A. Nowak, W. Duchnik, Ł. Kucharski, J. Rokicka, A. Klimowicz and Z. Czech, *Int. J. Mol. Sci.*, 2021, **22**(21), DOI: **10.3390/ijms222111840**.